YMTHE, Volume *31*

Supplemental Information

Reactive oxygen species-responsive nanocarrier ameliorates murine colitis by intervening colonic innate and adaptive immune responses

Xiangji Yan, Lingzhang Meng, Xingzhe Zhang, Zhichao Deng, Bowen Gao, Yujie Zhang, Mei Yang, Yana Ma, Yuanyuan Zhang, Kangsheng Tu, Mingzhen Zhang, and Qiuran Xu

Supplemental data

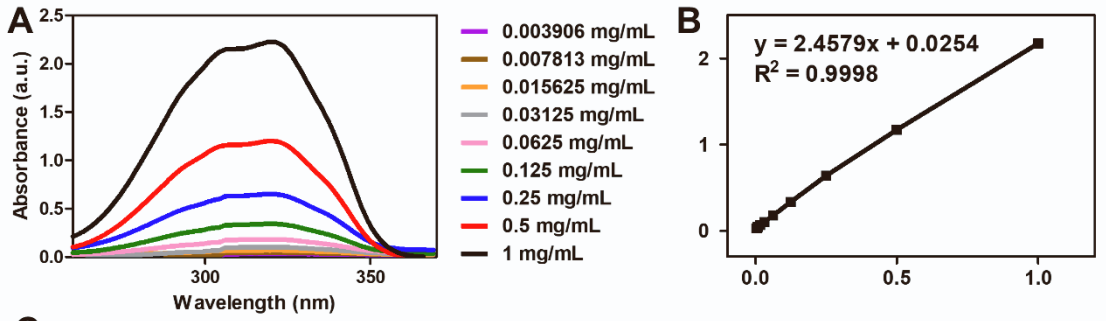

C

	Entrapment efficiency (EE%)	Loading capacity (LC%)
PSB@NP (2.5mg)	85.27%	3.74%
PSB@NP (5mg)	50.18%	3.38%
PSB@NP (7.5mg)	48.44%	3.02%
PSB@NP (10mg)	18.89%	1.36%

Figure S1. The entrapment efficiency and loading capacity of PSB in PSB@NPs were measured by a UV-vis spectrophotometer. (A) Absorption peaks of PSB with different concentrations. (B) The standard curve. (C) The entrapment efficiency and loading capacity of different dosages of PSB in PSB@NP.

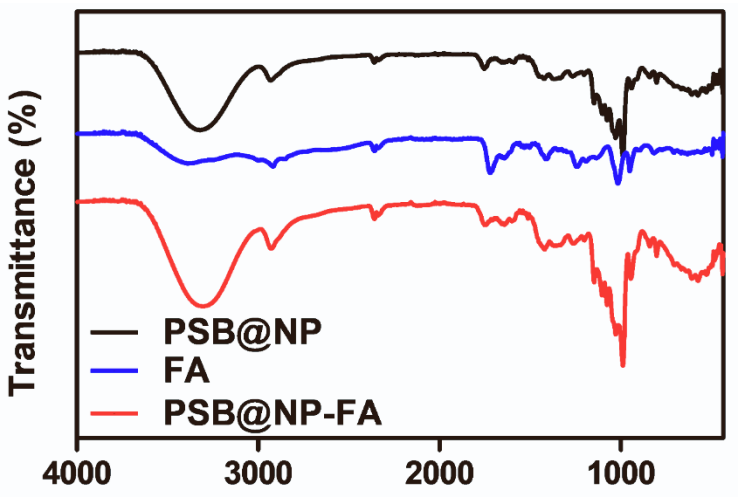

Figure S2. FTIR spectra of PSB@NP, FA and PSB@NP-FA.

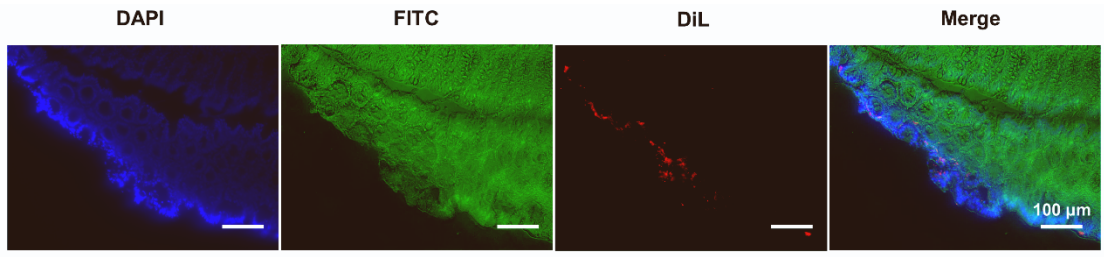

Figure S3. Frozen sections of colon tissues uptake with DiL labeled-NP. Phalloidin-FITC (green) represents actin and DAPI (blue) for nuclei. Scale bar: 100 μm.

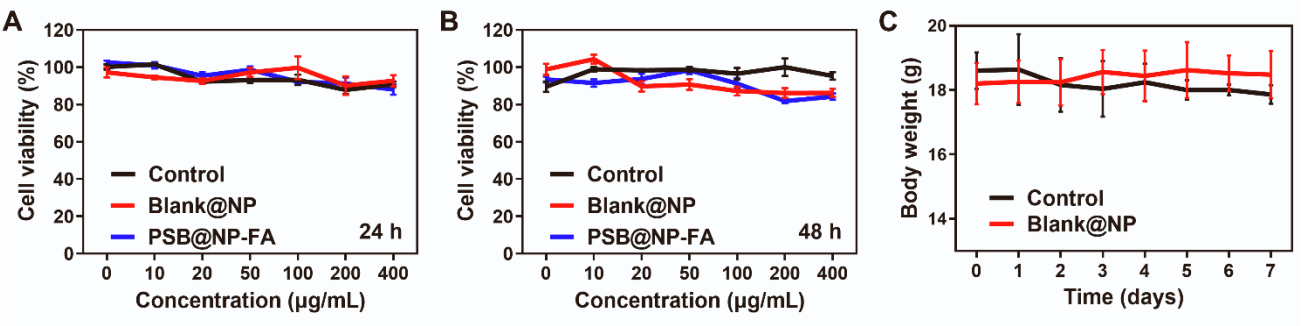

Figure S4. Biocompatibility of NP was assessed *in vitro* and *in vivo*. (A) *In vitro* cytotoxicity of different concentrations of Blank@NP and PSB@NP-FA in RAW 264.7 cells after incubating for 24 h and 48 h, as determined by MTT assay. (B) *In vitro* cytotoxicity of different concentrations of Blank@NP and PSB@NP-FA in RAW 264.7 cells after incubating for 48 h. (C) Daily changes in body weight of healthy mice treated daily for 7 days with Blank@NP or saline (n = 5).

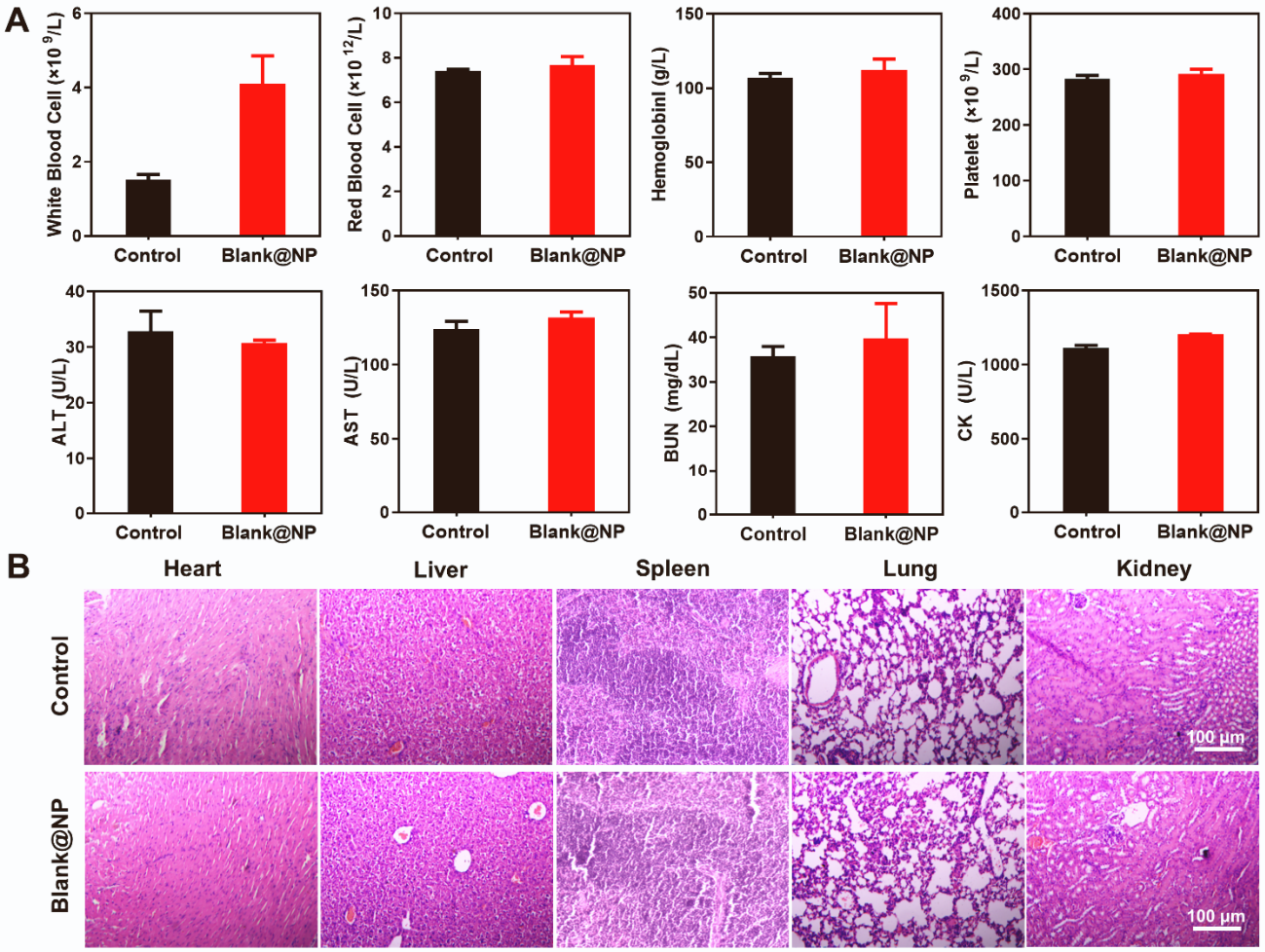

Figure S5. Biocompatibility evaluation of NP. (A) Biocompatibility evaluation was evaluated by analyzing hematology and biochemistry parameters, (n = 5). (B) Representative photomicrographs of H&E-stained sections of the major organs (heart, kidney, liver, lung, and spleen). Scale bar: 100 μm.

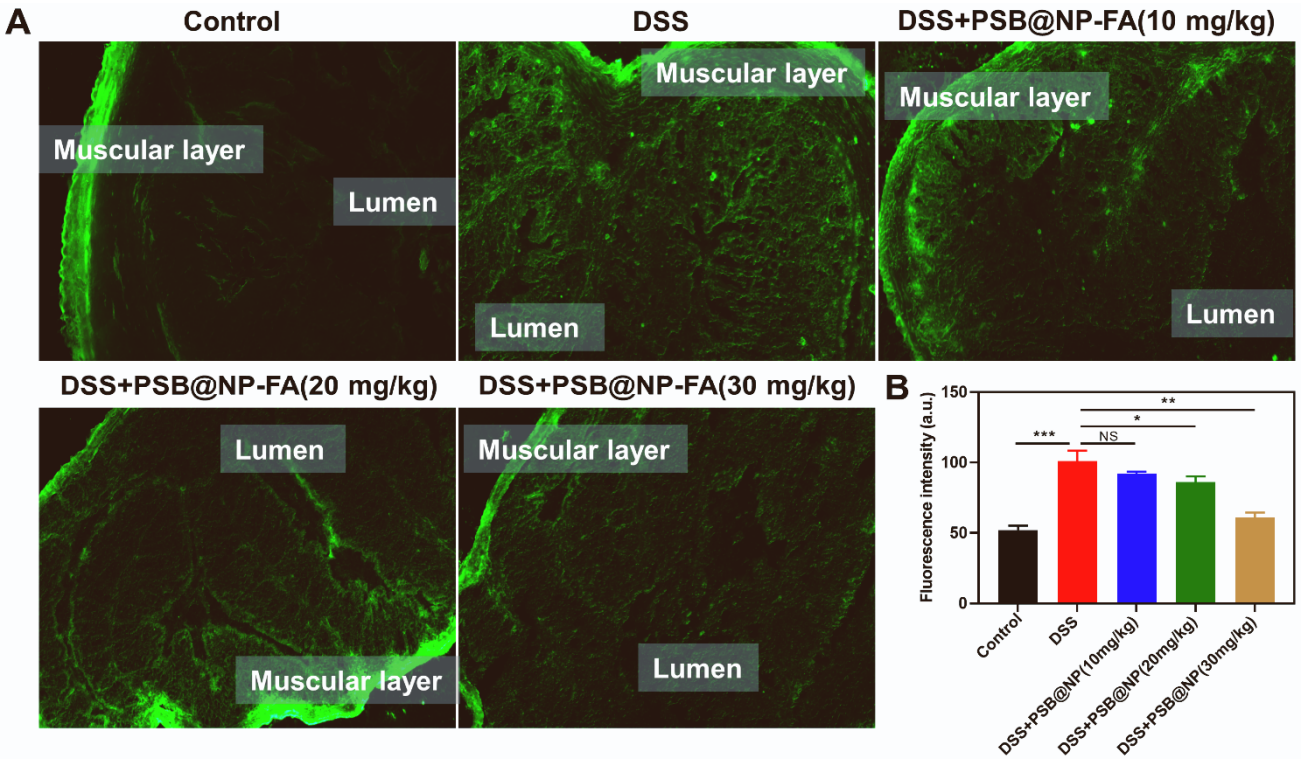

Figure S6. The level of ROS *in vivo* was detected by ROS probe DCFH-DA. (A) Fluorescence intensity of frozen sections of colon tissues in different treatment groups. (B) Histogram of fluorescence signal statistics of different groups.

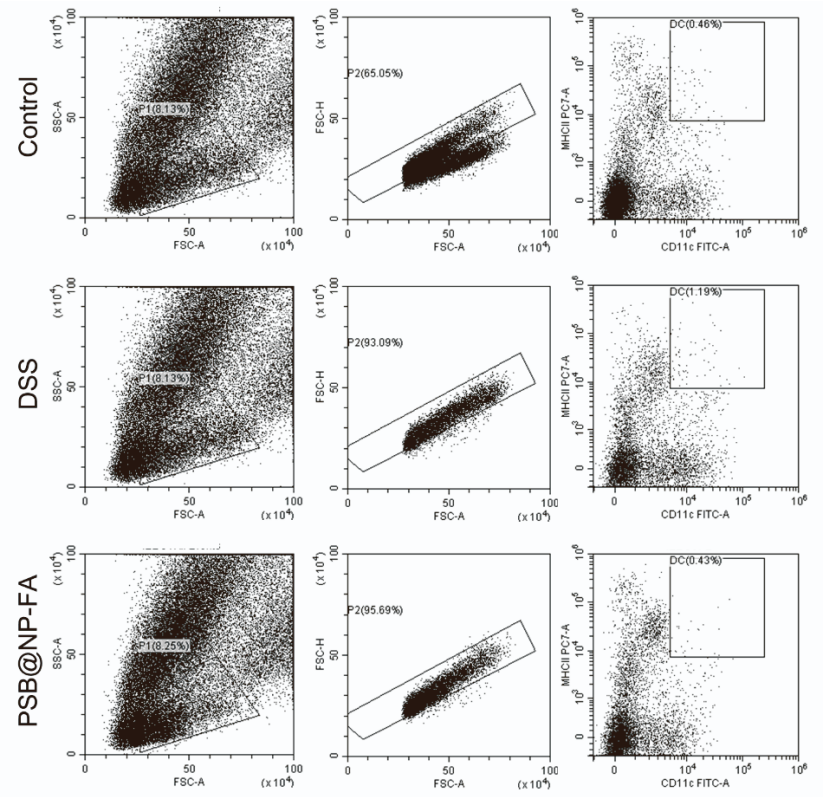

Figure S7. Scatter plots of Figure 5A.

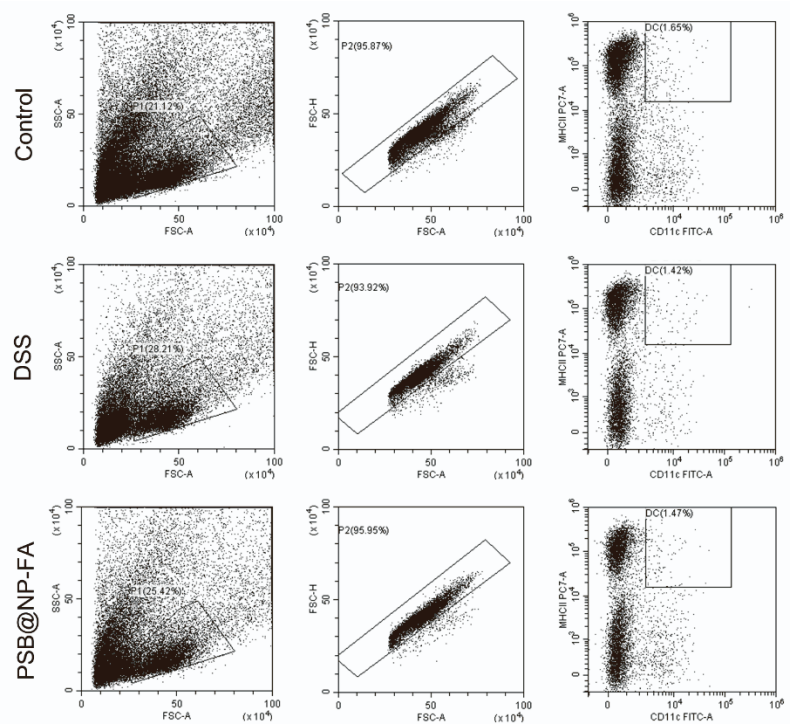

Figure S8. Scatter plots of Figure 5B.

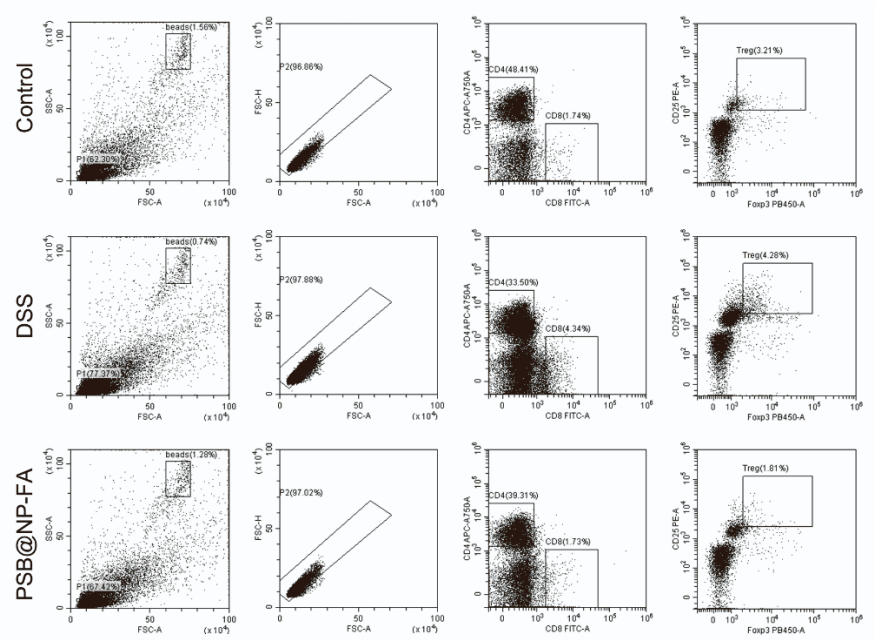

Figure S9. Scatter plots of Figure 6C.

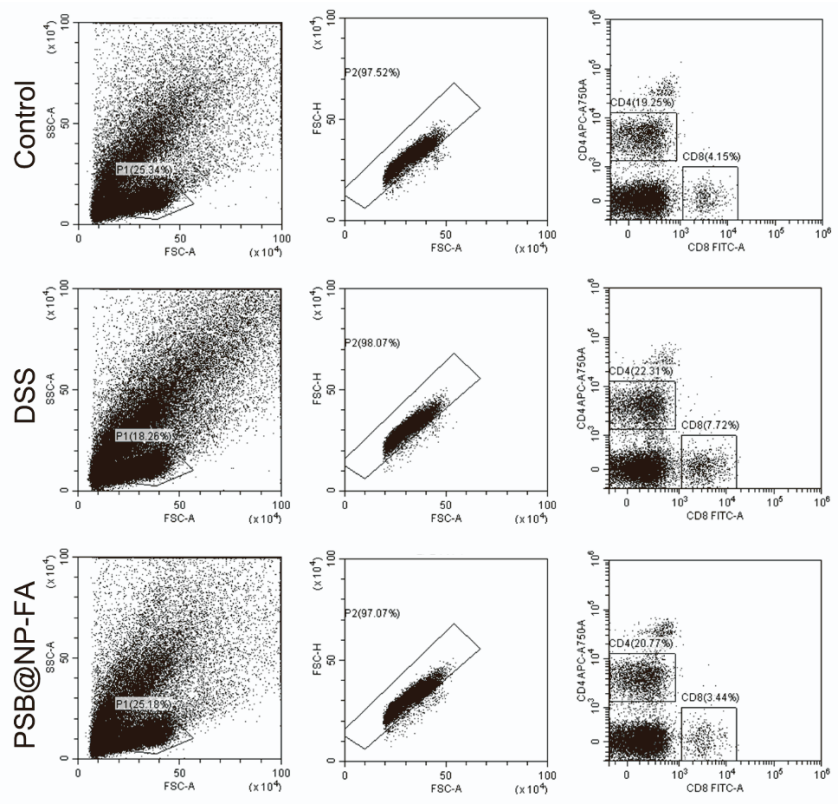

Figure S10. Scatter plots of Figure 6E.

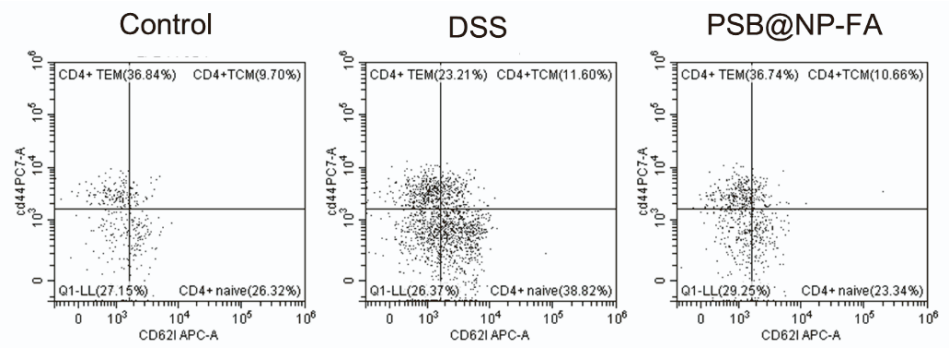

Figure S11. Scatter plots of Figure 6 FGH.

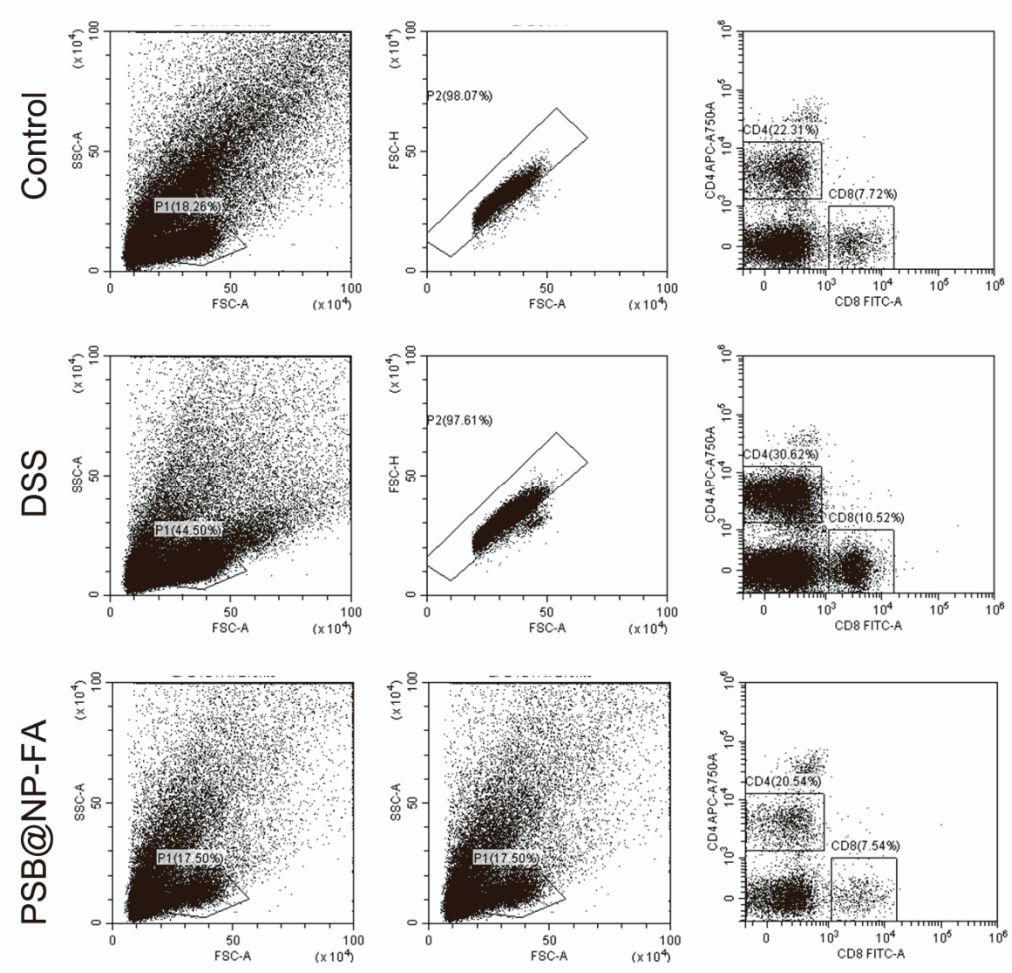

Figure S12. Scatter plots of Figure 6M.

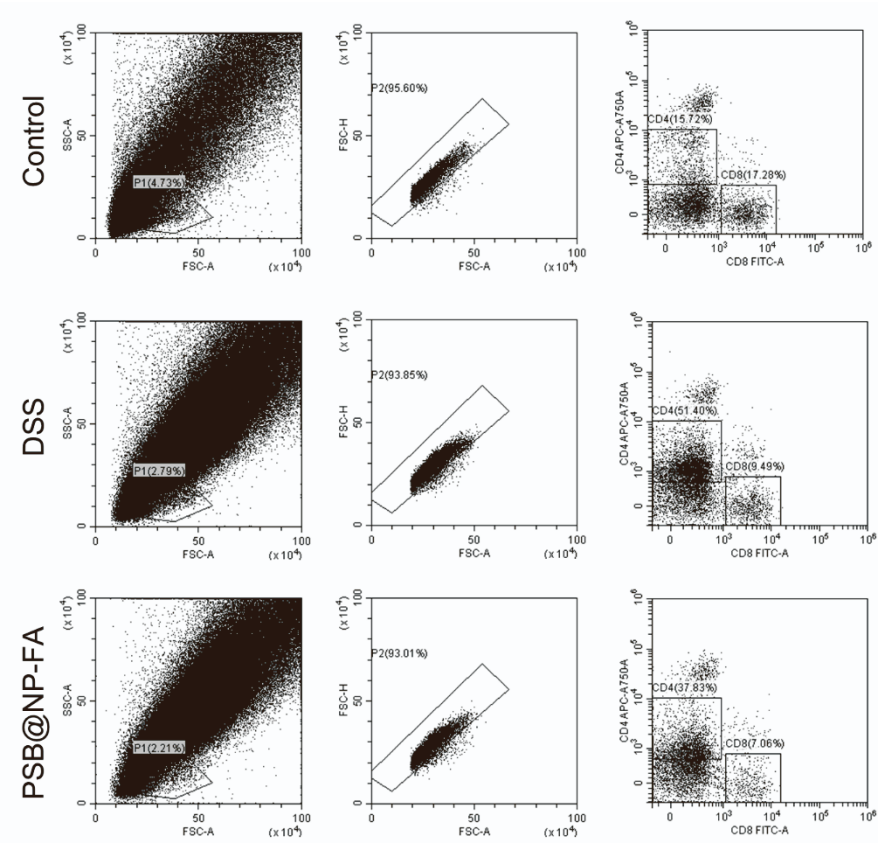

Figure S13. Scatter plots of Figure 6O.

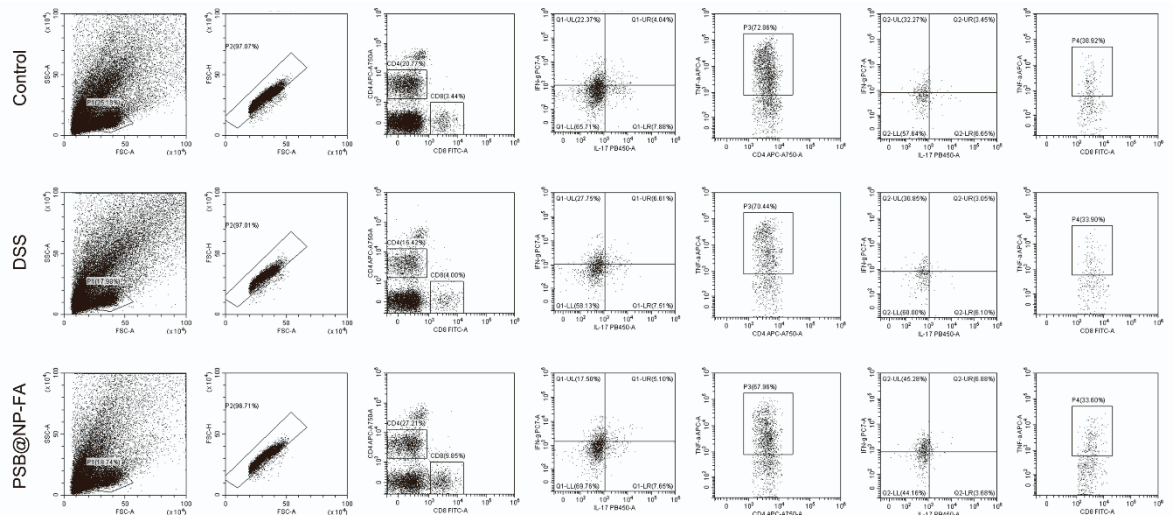

Figure S14. Scatter plots of Figure 7.

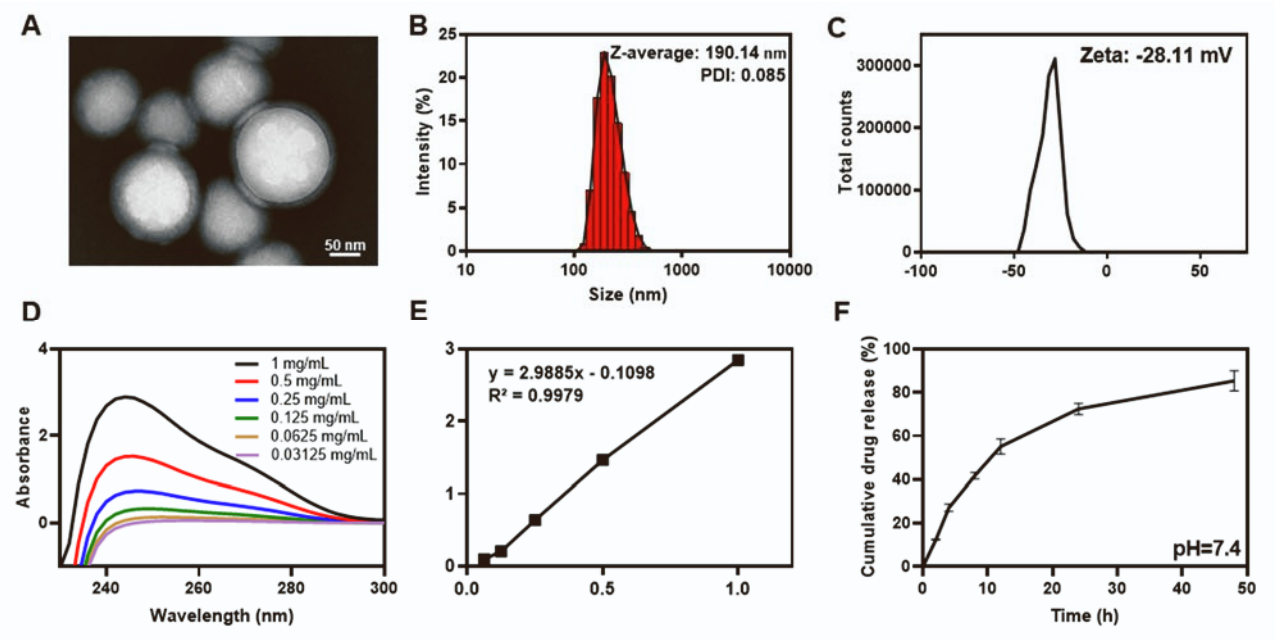

Figure S15. Characterization and *in vitro* drug-release profiles of DEX/PSB@NP-FA. (A) Representative TEM images of DEX/PSB@NP-FA. Scale bar: 50 nm. (B) Representative size distribution and PDI of DEX/PSB@NP-FA, (n=3). (C) Zeta potential of DEX/PSB@NP-FA, (n=3). (D) UV-vis absorption spectra of DEX with different concentrations. (E) The standard curve of DEX. (F) The release profile of DEX from PLGA (pH 7.4), (n=3).

Table S1. Primers used for Real-time PCR.

Gene	Forward primer (5'-3')	Reverse primer(5'-3')
TNF-α	AGGCTGCCCCGACTACGT	GACTTTCTCCTGGTATGAGATAGCAAA
IL-6	ACAAGTCGGAGGCTTAATTACACAT	TTGCCATTGCACAACTCTTTTC
IL-1β	TCGCTCAGGGTCACAAGAAA	CATCAGAGGCAAGGAGGA AAAC
IL-12	GCCAGTACACCTGCCACAAA	TGTGGAGCAGCAGATGTGAGT
IL-10	GGTTGCCAAGCCTTATCGGA	CTTCTCACCCAGGGAATTCA
36b4	TCCAGGCTTTGGGCATCA	CTTTATCAGCTGCACATCACTCAGA